Mapping the stability of perturbed two-planet systems using GPUs

J. Bédorf[a], C. Roedig[b], E. B. Ford[c]

[a]*Leiden Observatory, Leiden University, P.O. Box 9513, 2300 RA Leiden, The Netherlands*
[b]*Max-Planck Institut für Gravitationsphysik, Am Mühlenberg 1, D-14476 Golm, Germany*
[c]*University of Florida, 211 Bryant Space Science Center, Gainesville, FL 32611-2055, USA*

Abstract

We investigate the long-term orbital stability of two-planet systems, both in isolation and effected by external perturbations (e.g., a wide stellar binary companion). We perform direct N-body integrations of large ensembles of planetary systems using the `Swarm-NG` library and NVIDIA graphics processing units. We find that closely spaced planetary systems can be empirically stable when near mean motion resonances for Neptune or super-Earth-mass planets and that even for giant planets closely spaced systems can be stable for high orbital eccentricities. We also test how the volume of phase space which is apparently stable changes with the addition of an external perturber. For the systems we consider (restricted to coplanar orbits), we find that the volume of stable regions is only weakly affected by the presence of a wide binary companion of realistic mass.

Jeroen, TODO NOTE TO SELF. Maybe reverse the bar order of histograms, to put them in same order as all the other plots

Keywords: bla

1. Introduction

The long-term stability of planetary systems has long been an area of research. Activity has increased since the discovery of exoplanetary systems with multiple planets. Exoplanet searches have discovered over forty systems with multiple planets, mostly based on their radial velocity variations (Wright et al., 2009). While these systems are generally presumed to be stable (at least for a time comparable to the system age), some of the systems are tightly "packed", meaning that there are "nearby" qualitatively similar orbital solutions that are unstable on a much shorter timescale (Raymond et al., 2009; Barnes and Quinn, 2004). In several systems the orbital periods are near a 2:1 commensurability and the planets may participate in a 2:1 mean motion resonance (MMR), e.g., GJ 876 (Correia et al., 2010; Rivera et al., 2010), HD 82943 (Lee et al., 2006), Kepler-9 (Holman et al., 2010). In these systems, strong planet-planet interactions can be observed on an observable timescale. Of particular interest, two systems have been discovered in even more tightly packed configurations. The planets of HD 45364 appear to be in a 3:2 MMR (Correia et al., 2009) and those of HD 200964 in a 4:3 MMR (Johnson et al., 2010a). For giant planets, such tightly packed configurations are typically only stable if the planets are protected from close encounters by a MMR.

As exoplanet searches begin to discover less massive planets, the population of known exoplanet systems may grow to contain even more tightly packed planetary systems that are not participating in MMRs. If the actual population of planetary systems does not include systems which would be stable, then this could provide a clue to planet formation processes. In order to turn exoplanet discoveries into tests of planet formation models, it is important to understand the range of masses and orbitals that are possible (i.e., long-term stable). Only then can we ask questions such as whether the known systems are consistent with a sample from all possible orbital configurations.

This study represents a first step towards understanding what types of planetary systems could be long-term stable. For simplicity, we focus on two-planet systems. For sufficiently separated systems, some configurations are provably Hill stable (Gladman, 1993). However, some systems that are not provably Hill stable may still be stable. We use direct N-body integrations to identify such systems. The Hill stability criterion is only applicable to isolated systems. Therefore, we also investigate the stability of two-planet systems under the presence of external perturbations (e.g., a wide stellar binary). We investigate how large a region of phase space near each of several MMRs is long-term stable. We also investigate which MMRs are surrounded by nearby, stable orbital solutions.

2. Method

2.1. Planetary integrators

Numerous numerical integration techniques have been applied to study planetary systems. For long–term integrations, it is important to use an algorithm that is either symplectic, time reversible, or both. The mixed–variable symplectic method is usually the method of choice for long-term integrations to test for orbital stability. In this study, we use a time–symmetrized 4th order Hermite integrator which has been optimized for planetary systems (Kokubo et al., 1998; Kokubo and Makino, 2004). This integrator is computationally efficient and provides high accuracy for long-term integrations. In particular, we use the `Swarm-NG` package for integrating an ensemble of few-body systems in parallel with a graphics processing unit (GPU).

2.2. Graphics Processing Units

There is a great demand for computational power in the fields of astronomy and astrophysics, (e.g., large simulations, Monte Carlo studies of large parameter spaces, analysis of large observational data sets). Often a study is limited to a certain number of bodies (N) that can be integrated in reasonable time. In the case of observational research, there may be a limit to the amount of data that can be processed within reasonable time. Fortunately, astronomers are not the only ones that are always in need of computational power. In the fields of computer graphics and gaming computational power is also in high demand. Indeed, computer gaming can drive the development of the computer processor industry, as gamers want more special effects and even higher levels of graphical detail. While rendering those details requires a lot of computational resources, most of the calculations involved are relatively simple and can be performed in parallel. This has shaped the development of graphics processing units (GPUs). They are highly parallelized, so as to perform the rendering methods much faster than if the rendering tasks were performed by a standard processor (CPU). Recently, the performance of GPUs has increased more rapidly than the performance of CPUs, causing the GPUs to have a theoretical peak performance more than a magnitude higher than top-of-the-line CPUs. Fortunately, GPU developers have extended the capabilities of the GPU making it possible for scientists to harness the power of GPUs for science (Buck et al., 2004). At first programming GPUs had to be done in a language which was designed for rendering computer graphics and was not very efficient for other non-game related problems. In 2006 NVIDIA Corp. introduced the Compute Unified Device Architecture (CUDA) programming language and compatible GPUs[1]. This made it much more efficient to use the GPU as a co-processor to offload computational heavy parts of the algorithm and more practical to program them for scientific computation. Today GPUs offer over 1 TFLOP in single precision and 515 GFLOP of double precision performance[2]. This allows the GPU to outperform the CPU by orders of magnitude (in either single or double precision). Apart from more computational power the GPUs also have a higher memory bandwidth between the memory and the processing unit than CPUs. This makes the GPUs also suitable for algorithms that require a lot of data processing.

The first serious use of the GPU in astronomy was for direct N-body simulations (Portegies Zwart et al., 2007; Hamada and Iitaka, 2007; Belleman

[1] http://www.nvidia.com/cuda

[2] The NVIDIA Tesla C1060 that we have used in this projects has a double precision performance of 78 GFLOP.

et al., 2008; Gaburov et al., 2009). For large N, these simulations are highly parallel by nature and can make excellent use of the GPU to compute the gravitational force. However the in these papers discussed techniques are not applicable to small N-body systems which require an alternative approach which will be described in §2.4. Recently, other astronomy algorithms have been successfully ported to the GPU, including but not limited to: Gravitational Lensing (Thompson et al., 2010), hierarchical N-body methods (Gaburov et al., 2010; Bédorf et al., 2011), Adaptive Mesh methods (Schive et al., 2010) and radio astronomy signal convolution (Harris et al., 2008).

2.3. Hardware Used

The GPUs used for the simulations are NVIDIA Tesla C1060 GPUs. These cards have 78 GFLOPs of double precision performance and have an on device bandwidth of 102GBs. The cards are connected with the host system by a PCI-E x16 connection. The host has 16GB of internal memory and two AMD Opteron 2376 Quad-core processors.

2.4. Software

In this study, we use the `Swarm-NG` package [3] for integrating ensembles of few-body planetary systems in parallel with a GPU. With large N-body systems one can easily distribute the work over the processing units of the GPU; with small N this is not trivial since there is much less parallelism. `Swarm-NG` is specifically designed for such systems. Instead of breaking up one problem into parallel tasks, `Swarm-NG` integrates thousands of few-body systems in parallel. This makes `Swarm-NG` especially suited for Monte Carlo type of simulations where the same problem is run multiple times with varying initial conditions and/or model parameters.

The implementation of `Swarm-NG` is such that the problem setting and configurations are loaded on the GPU. Then the configurations are simulated in time on the GPU without intervention of the host system. When the simulation is finished (or the memory buffers are full), the results are written back to the host. Therefore, the performance of the software depends solely on the GPUs used. The data analysis is performed on the CPU after the simulations are complete.

3. Initial Conditions

3.1. Configurations

The main aim of this study is to determine the shape and size of the stable regions of parameter space for tightly packed two-planet systems. We are particularly interested in the potential of stable orbital solutions near MMRs. For three-body systems, there are three masses and eighteen coordinates required to describe each set of initial conditions. Six of these can be eliminated without loss of generality by shifting to the center of mass frame. Thus, we specify the initial conditions for the two planets, but not the star. Two more parameters can be eliminated by scaling of system masses by the central mass ($m_\bigstar = 1M_\odot$) and distances by the initial semi-major axis of the inner planet ($a_1 = 1$ AU) for point masses where collisions are ignored. Another four parameters can be eliminated for coplanar systems ($i_1 = i_2 = \Omega_1 = \Omega_2 = 0°$, where i as the inclination and Ω is the longitude of the ascending node). Still, methodically exploring an eight-dimensional phase space is quite challenging. Thus, we choose to perform Monte Carlo exploration of a seven dimensional phase space (a_2/a_1, e_1, e_2, ω_1, ω_2, M_1, and M_2) for each of several sets of planet masses (m_1 and m_2). Here e is the initial orbital eccentricity, ω is the initial argument of periapses, and M is the initial mean anomaly. Subscripts refer to the planets according to their initial distance to the central star. Except where otherwise noted, each of these parameters was varried uniformly over it's allowed interval: $a_2 \in [1.0, 2.0]a_1$, $e \in [e_{\min}, e_{\max})$, $\omega \in [0, 2\pi)$, $M \in [0, 2\pi)$). We choose both planets to have similar masses, either close to Jupiter-mass, Neptune-mass or super-Earth-mass (3.5 Earth masses). The respective masses of the planets are varied around the given mass-ratio in a 1% interval. For each ensemble, we integrate $N = 11520$ systems and integrate them in time for over one million years.

Our simulations are subdivided in the *basic*, the *perturbed* and the *special* setups. In addition to the

[3] http://www.astro.ufl.edu/∼eford/code/swarm/

above stated, we first describe the basic setup. For three sets of simulations[4], (r1aX, r2bX, r3cX), we keep the ranges of the eccentricities very low to study the stability of nearly circular systems. In order to study the influence of the initial eccentricity, we then increase $e_{\max}$ for e_1 and e_2 to 0.1 in runs r1aY, r2bY, r3cY and to 0.5 in runs r1aZ, r2bZ, r3cZ. The results of the *basic* runs are shown in Fig. 3 with the exception of the very low eccentricity runs, since they do not show any interesting features.

In the *perturbed* simulations, we investigate how the stability regions would be affected by the influence of a distant perturbing star. For these simulations, the external perturber has a semi-major axis of $a_{pert} = 100$ and an eccentricity of $e_{pert} = 0.3$. Its orbit lies in the same plane as the planets (i.e., $i_{pert} = 0$ and $\Omega_{pert} = 0$). And the orbital phase is randomized (ω_{pert} and $M_{pert} \in [0,360]$ deg). We consider multiple stellar masses ($m_{\rm pert}$ = 1.0, 20 and 50). The motivation for choosing such a high mass for the pertuber in r6aYp50_03 is to see whether there is any point where, independent of the unperturbed IC, the system is destabilized completely by the external mass. The results from the *perturbed* runs are shown in Fig. 4.

In the case of the *special* simulations, we fix the initial pericenter angles and mean anomalies to search for more detailed phase space structure when we reduce the number of degrees of freedom for the initial conditions. The results from the *special* runs are shown in Fig. 5.

The initial conditions for each of our ensembles can be found in Table 1.

3.2. Data processing

During the course of integrations Swarm-NG logs to disk snapshots of each system at specificied times. This allows us to plot orbital elements versus time or to determine the distance between the star and the planets. We use these snapshots to identify which initial conditions are manifestly unstable during the course of our integration. In particular, we identify a system as unstable if either of the following two criteria are met:

- Close encounters between planets
- Large changes in star-planet distance

Close encounters between planets We test for two planets having a close encounter, defined to occur when the two planets come within one Hill radius of each other. According to Hill (1878), the Hill radius is given by

$$R_{Hill} = a\left(\frac{m_{planet}}{3m_\bigstar}\right)^{\frac{1}{3}} \tag{1}$$

Large changes in star-planet distance We calculate the distance between each of the planets and the star to check if mutual planetary perturbations have caused either planets to have been ejected from the system or scattered onto an orbit with a significantly different semi-major axis. For each snapshot we compute the current distance between each planet and the star. If any of the planets is further than 10 AU we declare the system as unstable, as the orbits have obviously been significantly changed.

Once the snapshots have been processed we end up with a list of stable and a list of unstable initial conditions. These lists are then used to create stability maps (e.g., Fig. 2) and for performing statistics.

4. Results

Here we present the results of our stability analysis of the previously described simulations. All simulations are performed using the Swarm-NG software package and its hermite_gpu integrator.

The nomenclature of our runs corresponding to their initial conditions is listed in Tab. 1.

All simulations have been run for 10^6 years with a time-step of 0.003 year (1.16 days) per step, which proves to be long enough to get good statistics on

[4]The naming of the simulations is as follows: The first character is always ‘r’, the number indicates the global configuration, followed by a character that indicates the mass of the planets (a=Jupiter mass, b=Neptune mass and c=super-Earth mass). Then comes a character indicating the eccentricity range (X= $\in [10^{-4}, 10^{-3}]$, Y=$\in [0.15, 0.5]$ and Z=$\in [0.05, 0.15]$). If the configuration contains a perturber this is indicated with the ‘p’ directly followed by the mass of the perturber and the eccentricity. The last number indicates the semi-major axis of the perturber, if this is not indicated it is 100AU.

Name	Mass ratio	e_1 e_2	ω_1 ω_2	M_1	M_2	m_{pert}	M_{pert} ω_{pert}	e_{pert}	a_{pert}
r1aX	10^{-3}	$\in [10^{-4}, 10^{-3}]$	$\in [0,360]$	$\in [0,360]$	$\in [0,360]$	-	-	-	-
r1aY	10^{-3}	$\in [0.05, 0.15]$	$\in [0,360]$	$\in [0,360]$	$\in [0,360]$	-	-	-	-
r1aZ	10^{-3}	$\in [0.15, 0.5]$	$\in [0,360]$	$\in [0,360]$	$\in [0,360]$	-	-	-	-
r1aZp20_01	10^{-3}	$\in [0.15, 0.5]$	$\in [0,360]$	$\in [0,360]$	$\in [0,360]$	20	$\in [0,360]$	0.1	100
r1aZp02_03	10^{-3}	$\in [0.15, 0.5]$	$\in [0,360]$	$\in [0,360]$	$\in [0,360]$	2.0	$\in [0,360]$	0.3	100
r2bX	5.10^{-5}	$\in [10^{-4}, 10^{-3}]$	$\in [0,360]$	$\in [0,360]$	$\in [0,360]$	-	-	-	-
r2bY	5.10^{-5}	$\in [0.05, 0.15]$	$\in [0,360]$	$\in [0,360]$	$\in [0,360]$	-	-	-	-
r2bZ	5.10^{-5}	$\in [0.15, 0.5]$	$\in [0,360]$	$\in [0,360]$	$\in [0,360]$	-	-	-	-
r2bZp20_01	5.10^{-5}	$\in [0.15, 0.5]$	$\in [0,360]$	$\in [0,360]$	$\in [0,360]$	20	$\in [0,360]$	0.1	100
r2bZp02_03	5.10^{-5}	$\in [0.15, 0.5]$	$\in [0,360]$	$\in [0,360]$	$\in [0,360]$	2.0	$\in [0,360]$	0.3	100
r3cX	10^{-5}	$\in [10^{-4}, 10^{-3}]$	$\in [0,360]$	$\in [0,360]$	$\in [0,360]$	-	-	-	-
r3cY	10^{-5}	$\in [0.05, 0.15]$	$\in [0,360]$	$\in [0,360]$	$\in [0,360]$	-	-	-	-
r3cZ	10^{-5}	$\in [0.15, 0.5]$	$\in [0,360]$	$\in [0,360]$	$\in [0,360]$	-	-	-	-
r3cZp20_01	10^{-5}	$\in [0.15, 0.5]$	$\in [0,360]$	$\in [0,360]$	$\in [0,360]$	20	$\in [0,360]$	0.1	100
r3cZp02_03	10^{-5}	$\in [0.15, 0.5]$	$\in [0,360]$	$\in [0,360]$	$\in [0,360]$	2.0	$\in [0,360]$	0.3	100
r1aYp02_03_50	10^{-3}	$\in [0.05, 0.15]$	$\in [0,360]$	$\in [0,360]$	$\in [0,360]$	2.0	$\in [0,360]$	0.3	50
r1aYp02_03_20	10^{-3}	$\in [0.05, 0.15]$	$\in [0,360]$	$\in [0,360]$	$\in [0,360]$	2.0	$\in [0,360]$	0.3	20
r4aY	10^{-3}	$\in [0.05, 0.15]$	0,0	0	0	-	-	-	-
r5cY	10^{-5}	$\in [0.05, 0.15]$	0,0	0	180	-	-	-	-
r6aYp50_03	10^{-3}	$\in [0.05, 0.15]$	0,0	0	0	50	$\in [0,360]$	0.3	100

Table 1: List of the simulations with their respective values or intervals from which the initial conditions were generated in a Monte–Carlo fashion. Subscripts 1 or 2 refer to the inner and outer planet, repectively; *pert* refers to the external perturber.

Resonance	a_1/a_2	a_2
5:2	0.54288	1.84203
2:1	0.62996	1.58740
5:3	0.71138	1.40572
3:2	0.76314	1.31038
4:3	0.82548	1.21142
5:4	0.86177	1.16040
1:1	1.00000	1.00000

Table 2: List of numerical values of the expected resonances.

the stability regions, since most of the systems go unstable before 10^5 years and are stabilized by 10^6 years. In Fig. 1 we show the number of systems stable over the course of the simulation. Since we only take snapshots every ~ 4000 years, we have to determine the moment of unstability by the velocity of the escaping planet(s). This is not always possible and then the moment of unstability is set at the time of the snapshot, which explains the sometimes large drops in the number of stable systems.

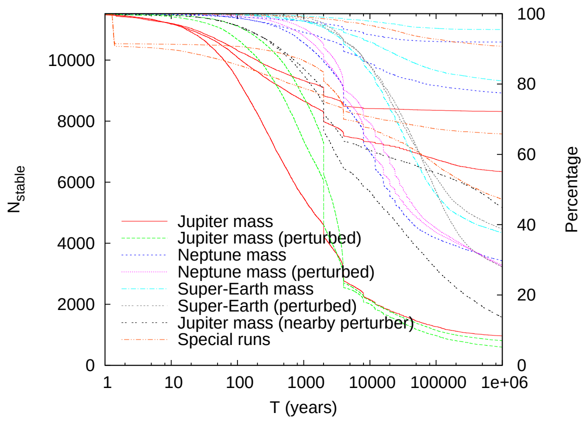

Figure 1: Number of systems stable over the course of the simulation. The x-axis indicates the time in years since the start of the simulation (in logscale). The y-axis shows the number of systems stable. Each line represents one of our configurations as specified in Tab. 1 and starts with 11520 systems at T=0.

To determine which parameters had the most influence on the stability of the systems we conducted a Pearson correlation test for the parameters that we varried (i.e., e_1 against ω_1, e_1 against a_2, ω_1 against ω_2, etc.). This was done for both stable and unstable initial conditions. For both sets and for all parameter combinations the Pearson correlation coefficient was near zero.

Since the Pearson correlation did not give a conclusive method to compare the systems, we checked for structure by plotting each parameter against all other parameters. None of the combinations showed sign of structure, except when we plot a_2 against e_1 or against e_2. In Fig. 2 we plot a selection of the stable and unstable systems of simulation `ra1X`. The selection is based on the semi-major axis of the second planet and only shows the systems where $a_2 = [1.2, 1.4]$. In the Figure we can see that there is a sharp transition between unstable ($a_2 = [1.2, 1.3]$) and stable ($a_2 = [1.3, 1.4]$) systems, but within the stable and unstable regions the points are distributed at random. We see the same effect in the other system configurations. Therefore in future plots we only plot the stable systems with on the x-axis the semi-major axis of the second planet (a_2) and on the y-axis the combined eccentricities of the planets ($\sqrt{e_1^2 + e_2^2}$). Note that this method will not evenly distribute the stable systems along the y-axis, but rather makes the center of the plots more dense than the top and bottom. For our analysis this is not important since we focus on the horizontal distribution and the overal effect of the chosen eccentricity range.

The outcome of selected simulations is shown in Figures 3, 4, 5 and Tab. 3. In the Figures we show the stable initial conditions. In the same figures the red line shows the normalized cumulative distribution of stable systems for the simulation and the green/shaded underlayed region is used for computing percentages in the histograms of §5. In the Table we list the percentage of systems that where stable at the end of the simulation.

In order to go systematically through the different sets of initial conditions (*ICs*), we will first discuss the overall effect of the *ICs*. Then, we will identify the presence and strength of the expected resonances, as given in Tab. 2. At last, we comment on the systematic differences in the resonance appearances in the different configurations.

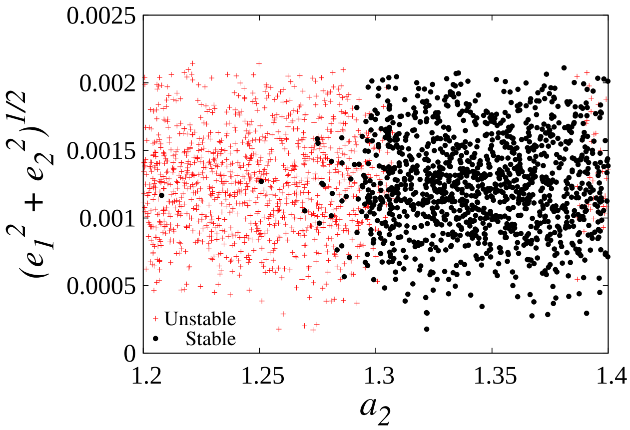

Figure 2: Stable and unstable initial conditions in one figure. We show a selection of `r1aX` where $a_2 = [1.2, 1.4]$. The x-axis shows a_2 the y-axis the combined eccentricities of the planets ($\sqrt{e_1^2 + e_2^2}$). The stable system are indicated by the black dots, the unstable systems by the red crosses.

Closely packed systems more stable for higher e: Looking at `r1aY, r2bY, r3cY` (Fig. 3(a) to 3(c), bottom panels) we see the behavior of the systems with very low initial e, we find a clear instability strip after the 1:1 MMR, with a wide gap for Jupiters and a small one for the lower mass planets. The instability strip is nearly vertical, meaning that the influence of the small e is negligible. In Fig. 3(a) to 3(c) (top panels), we find the influence of the eccentricity increasing as the boundary between stable and unstable systems is now merging together, making the gap disappear while the population of stable systems is thinning out towards higher e.

Phase-aligned orbits favour 5:4 MMR: Comparing Fig. 5(middle) with Fig. 3(a), we find that the prominence of resonances is significantly affected by the fixed initial orbital phases. The 1:1 MMR for the Jupiters is completely depopulated whereas the 5:4 MMR is clearly favoured for planets of aligned initial phase. The disappearance of the 1:1 MMR is easy to understand, since the planets would initially be extremely close to each other rather than near the leading/trailing Lagrange points.
In the anti-aligned case of `r5cY` (Fig. 5 top), we find

Name	stable after 10^6 y
`r1aX`	72%
`r1aY`	55%
`r1aZ`	8%
`r1aZp20_01`	5%
`r1aZp02_03`	7%
`r2bX`	92%
`r2bY`	77%
`r2bZ`	30%
`r2bZp20_01`	28%
`r2bZp02_03`	28%
`r3cX`	96%
`r3cY`	81%
`r3cZ`	38%
`r3cZp20_01`	28%
`r3cZp02_03`	39%
`r1aYp02_03_50`	45%
`r1aYp02_03_20`	14%
`r4aY`	66%
`r5cY`	91%
`r6aYp50_03`	47%

Table 3: Percentage of systems stable in each run after 10^6 years. For the configuration of each run see Tab. 1.

that the 1:1 MMR is stable. The gap between 1:1 and 5:4 is narrowed, compared to `r3cY` (Fig. 3(c)) and the stability of all other configurations is more evenly distributed over the shown parameter-space; resonances near any other MMR are not visible.

Carving out of the 5:3 MMR in the presence of perturbers: We generally find that the effect of the external perturber is remarkably small, even for high perturbing masses. In the lightly perturbed runs `r1aZp02_03`, `r2bZp02_03` and `r3cZp02_03` (Fig. 4) we hardly see any difference to their related runs `r1aY`, `r2bZ` and `r3cZ` (Fig. 3). However, in these runs, the perturbing mass is modest, $m_{pert} = 2$, and its separation, $a_{pert} = 100$, very large. Keeping the separation of the perturber fixed to $100AU$, while increasing its mass to $20M_\odot$ only shows marginally more destabilization: The more heavily perturbed runs `r1aZp20_01`, `r2bZp20_01` and `r3cZp20_01` show, in comparison to `r1aY`, `r2bZ` and `r3cZ`, an increasing depletion of the 5:3 MMR for Jupiters and a destabilization of highly eccentric orbits for the super–earth mass planets. However, for Neptunes, no measurable difference is visible. Placing the perturber of mass $m_{pert} = 2$ closer ($a_{pert} = 50$) has slightly more effect as seen in `r1aYp02_03_50` where the 5:3 MMR is clearly depopulated. Placing it even closer ($a_{pert} = 20$) finally changes the picture drastically. In run `r1aYp02_03_20` (Fig. 4(b) bottom) the stable islands have clearly moved away from the position expected for them for the unperturbed system. Tightly packed configurations are completely depleted whereas some of the low eccentricity systems can survive on very wide separations. Remarkably, all MMRs 5:4, 4:3, 5:3, 2:1 and 5:2 are carved out, rather than providing stability. This is confirmed in the phase-aligned run `r6aYp50_03` (Fig. 5, bottom), in which a perturber of unrealistically high mass $m_{pert} = 50$ is placed at a large distance $a_{pert} = 100$. The effect of the perturber is weaker than in the previous case, which is to be expected. However, the carving out of the 5:4, 4:3 and 2:1 MMR remains clearly visible, whereas the depopulation of the 1:1 MMR stems from the alignment of the orbits rather than from the presence of a perturber. In this aligned configuration, the 5:3 MMR is not clearly carved out;

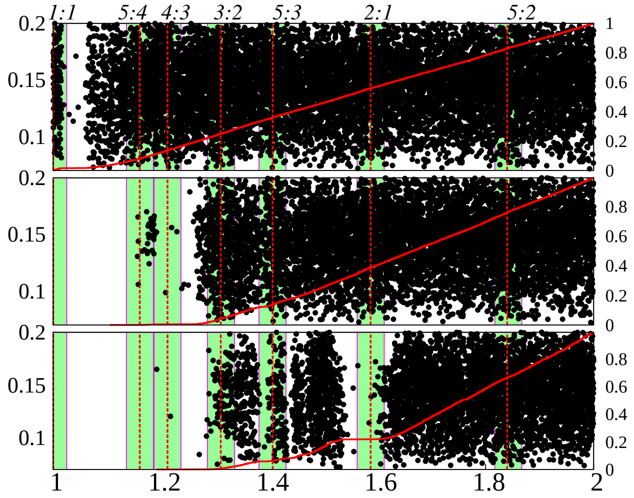

Figure 5: The stable systems of the *special* runs (see Tab. 1 for details). Top: SuperEarths (anti-aligned) `r5cY`, Middle: Jupiters (aligned) `r4aY`, Bottom: Jupiters (aligned and heavily perturbed) `r6aYp50_03`. The x-axis shows the semi-major axis of the second planet (a_2) and the y-axis the combined eccentricities of the planets ($\sqrt{e_1^2+e_2^2}$). The red line shows the normalized cumulative distribution of stable systems with labels on the right y-axis. The underlayed green/shaded region is used for computing percentages in the histograms (c.f. §5).

bottom panel of Fig. 5 rather shows two surrounding depletion strips.

To quantitatively summarize the results, we determine the significance of the stability zones as seen in Figs. 3, 4 and 5. We assign a system to a resonance region if a_2 lies within 0.025AU of the nominal location of the MMR, based on Kepler's law. Then we calculate the relative number of stable systems in each region compared to the total number of stable systems. This is to give an overview, whereas the accurate cumulative population is always depicted as the red solid line in Figs 3, 4 and 5. For clarity, the selected resonance regions are underlayed in green/shaded. In Fig. 6, we then plot the relative population of these green areas using histograms.

5. Discussion

Generally, we observe less stability for higher planet masses, which is due to the increasingly chaotic behaviour of the total system (**is it?**). Given the overview in Fig. 4 we clearly see that for the low mass planet systems (Figs. 6(e), 6(f), 6(h), 6(i), 6(k), 6(l)), the stability of the closely packed configurations is largely unaffected by a distant stellar companion, even for large stellar masses.

The survival fraction near the MMRs only changes for the 5:2 and 2:1 MMRs. This means that the perturber clearly only changes the shape of the gravitational potential at large distances whereas the central star dominates for closely packed configurations.

In contrast the behaviour of the systems with giant planets and small eccentricities is quite different, as depicted in Figs. 6(a), 6(g), 6(j), 6(m) the population of the 5:2, the 3:2 and the 1:1 MMR is virtually constant under the influence of a weak perturbation. It is clear to see that the heavy systems cannot be stable on the closely-packed MMRs 4:3 and 5:4 for low eccentric orbits. However, for highly eccentric orbits (e.g. Fig. 6(d)), even these closely packed systems can be comparably stable to wide configurations. This is not unexpected, because higher eccentricity will lead to a higher effective distance between the planets. Moreover, the effective cross–section for disruption will be decreased because of the larger speeds of the planets at close separations to the central star for higher eccentricities. Thus all systems that do not disrupt very early after periastron passage, because of counterrotation or unlucky phase-relations, will survive as long as the time-scale for some secular that destroys planets (?!) sets in.

Furthermore, for the Jupiters, we find that the population of the 5:3 MMR decreases with perturbation. It is interesting to observe that for low eccentricities and under perturbation, Jupiters can be closely packed on the 3:2 MMR only (exception: aligned orbits, see below). Whereas for higher eccentricities, the region around the 4:3 MMR provides additional stability. For wider configurations and high e, the 2:1 and 5:2 MMR both provide some stabilization.
In general, for the giant planets, an external perturber always leads to destabilization of all regions whereas for the low–mass systems the effect on the MMRs themselves is marginal, only on regions between res-

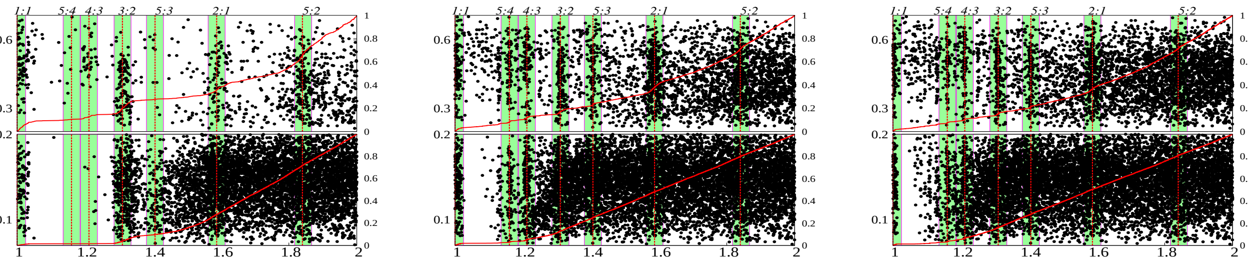

(a) *J*:`r1aZ` and `r1aY` (b) *N*:`r2bZ` and `r2bY` (c) *SE*: `r3cZ` and `r3cY`

Figure 3: Stable systems of a selection of the *basic* runs (see Tab. 1 for details). The x-axis shows the semi-major axis of the second planet (a_2) and the y-axis the combined eccentricities of the planets ($\sqrt{e_1^2+e_2^2}$). The red line shows the normalized cumulative distribution of stable systems with labels on the right y-axis. The configurations with eccentricity $\in [0.15, 0.5]$ are shown in the top panels and with eccentricity $\in [0.05, 0.15]$ in the bottom panels. The underlayed green/shaded region is used for computing percentages in the histograms (c.f. §5). *J* stands for Jupiter, *N* for Neptune, *SE* for SuperEarth

onances there is a clear tendency of destablization. **TODO refs to figures in lines above here**

The influence of the orbital phase is evident from Fig. 5 and is notably stronger than the influence of (weak) perturbation: For the Super–Earths, the anti-aligned configurations have an overall stabilizing effect as can be seen when we compare Fig. 6(c) and Fig. 6(p). It is easy to understand that for anti-aligned systems, it is much easier not to come within each others Hill radii and be disrupted, wherefore stability can be provided without MMRs. The fact, that the gap after the 1:1 MMR still persists stems from the fact, that **Magic?! Aliens?! Maybe...42! TODO! ...** For Jupiter, in the case of aligned orbits (cf. Figs. 6(n), 6(o), 6(q)) , the 5:3 MMR is strengthened even in the presence of a perturber, whereas the 1:1 MMR is completely unstable. The latter can easily be understood again because of the initial closeness of the planets around the 1:1 MMR. However, the strengthening of the 5:3 MMR must be due alone to the phase-alignment. In general, the phase alignment strengthens the stability of all giant-planet configurations (cf. Fig. 6(a) to Figs. 6(o),6(q)).

Comparing our simulations with Jupiter mass planets with recent studies of the system HD 200964, in which Johnson et al. (2010b) have found a 4:3 MMR with an eccentricity of both planets $e \sim 0.1$, we find less than 0.1% of low-eccentricity systems can be stable on the 4:3 MMR in our simulations (cf Fig 3(a)). Since, however, there are surviving configurations, we could not rule out such an interpretation. In comparison with the 24Sextans system, the eccentricity of which was determined to be $\sqrt{e_1^2+e_2^2} \sim 0.45$, we can easily support the 2:1 MMR configuration even if we consider an external perturbation being persent (cf. Fig.s 3(a), 4), which is reported in (literature).

6. Conclusion

In this paper we have mapped the stable regions of phase space for closely packed coplanar, two-planet systems. We find that pairs of giant planets are very rarely stable between the 3:2 MMR and the co-orbital region, even for nearly circular orbits. We find stable, closely packed configurations for the giant planets only favoured for highly eccentric orbits. The regions around the 2:1 and 3:2 MMRs have a significant volume of stable phase space for sizable eccentricities. The addition of a distance solar-mass coplanar binary companion does not significantly reduce the volume of stable phase space. Only for very large companion masses we found an increasing depletion of the 5:3 MMR.

We find that systems with low-mass planets can be much more tightly spaced than those with giant planets. In particular, there are even stable configurations inside the 5:4 MMR especially for highly eccentric orbits. The addition of a wide binary companion does not influence the close packed configurations of low-mass systems. A weak destabilization is

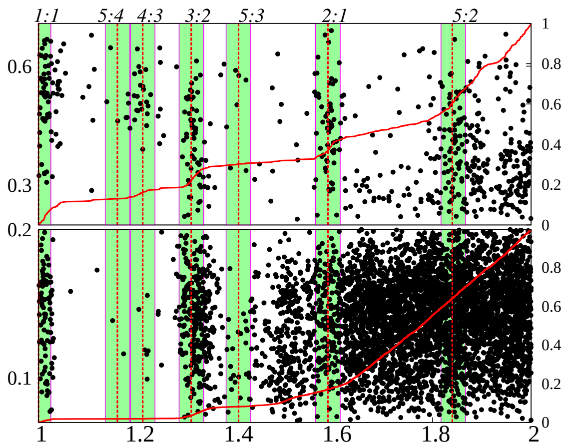

(a) Top: *J* with heavy distant perturber `r1aZp20_01`, Bottom: *J* with light perturber (closer) `r1aYp02_03_50`

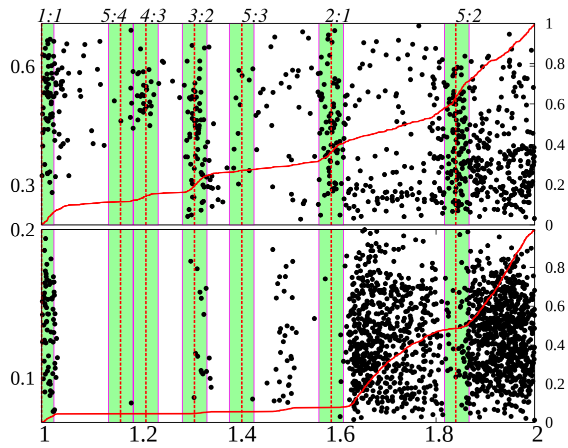

(b) Top: *J* with light distant pertuber `r1aZp02_03`, Bottom: *J* with light close perturber `r1aYp02_03_20`

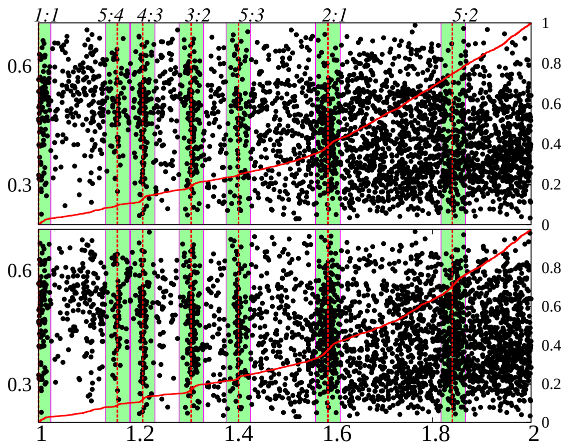

(c) Top: *N* with heavy distant perturber `r2bZp20_01`, Bottom: *N* with light distant perturber `r2bZp02_03`

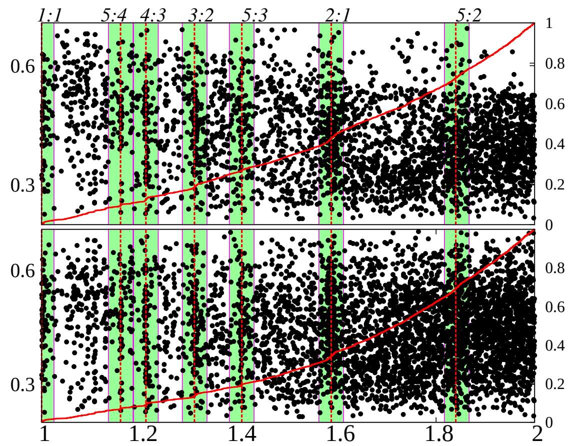

(d) Top: *SE* with heavy distant perturber `r3cZp20_01`, Bottom: *SE* with light distant perturber `r3cZp02_03`

Figure 4: The stable systems of the *perturbed* runs (see Tab. 1 for details). The x-axis shows the semi-major axis of the second planet (a_2) and the y-axis the combined eccentricities of the planets ($\sqrt{e_1^2+e_2^2}$). The red line shows the normalized cumulative distribution of stable systems with labels on the right y-axis. The underlayed green/shaded region is used for computing percentages in the histograms (c.f. §5). *J* stands for Jupiter, *N* for Neptune, *SE* for SuperEarth

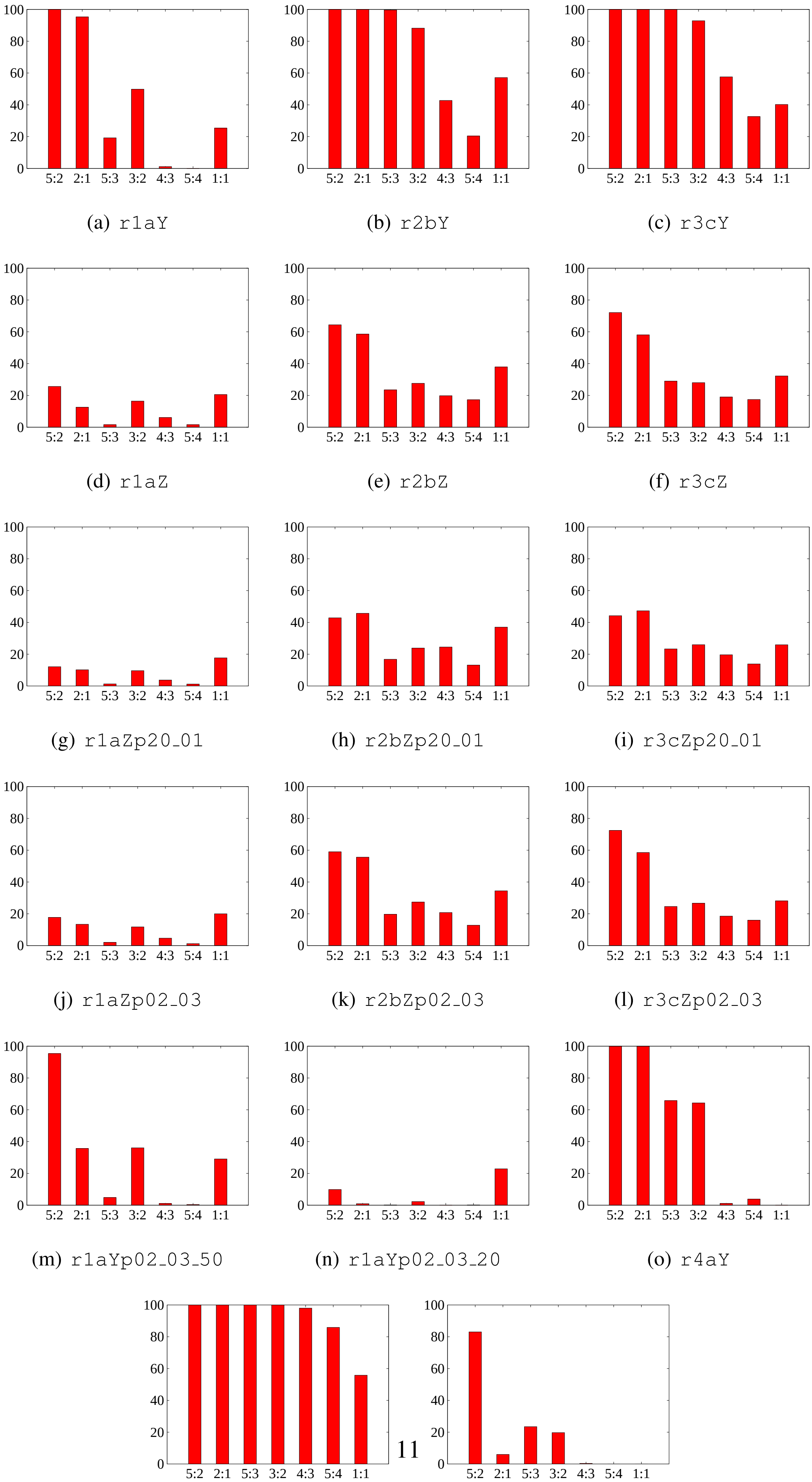

(a) `r1aY` (b) `r2bY` (c) `r3cY`

(d) `r1aZ` (e) `r2bZ` (f) `r3cZ`

(g) `r1aZp20_01` (h) `r2bZp20_01` (i) `r3cZp20_01`

(j) `r1aZp02_03` (k) `r2bZp02_03` (l) `r3cZp02_03`

(m) `r1aYp02_03_50` (n) `r1aYp02_03_20` (o) `r4aY`

(p) `r5cY` (q) `r6aYp50_03`

Figure 6: Histograms showing the percentage of systems which were stable over 10^6 years for each of several resonance regions.

only observed for widely spaced configurations with high eccentricity away from resonance.

This study has shown that with the currently available computational power (for example in the form of GPU clusters) it is practical to perform Monte Carlo type investigations of high-dimensional parameter space in reasonable time. This enables researchers to quickly determine regions of interest on which to focus in future studies. An example of this would be to define stability regions for various configurations of planetary systems. In this study, we focused on a clearly defined set of simulation parameters to study closely spaced systems in general. Future research could consider the effects of additional parameters (e.g., inclination, different mass ratios for the individual planets). Such studies can contribute to the study of extrasolar planetary systems, as they can quickly explore a large parameter space to identify stable orbital configurations.

Acknowledgement

We thank the Lorentz International Center for Workshops in the Sciences and the conference organizers for their hospitality and facilitating this study. The authors wish to thank Simon Portegies Zwart for helpful comments. We also thank Steve McMillan and Dejan Vinkovic for using their GPU clusters to execute the simulations. We thank Aaron Boley, Jianwei Gao, Mario Juric and Young In Yeo for their contributions to the `Swarm-NG` package. JB is supported by NWO grant #643.000.802. CR is supported by the International Max-Planck Research School. E.B.F was supported by NASA Origins of Solar Systems grant NNX09AB35G and NASA Applied Information Systems Research grant NNX09AM41G.

References

Barnes, R., Quinn, T., Aug. 2004. The (In)stability of Planetary Systems. ApJ 611, 494–516.

Bédorf, J., Gaburov, E., Portegies Zwart, S., Jun. 2011. A sparse octree gravitational N-body code that runs entirely on the GPU processor. ArXiv e-prints.

Belleman, R. G., Bédorf, J., Portegies Zwart, S. F., 2008. High performance direct gravitational n-body simulations on graphics processing units ii: An implementation in cuda. New Astronomy 13 (2), 103 – 112.
URL http://www.sciencedirect.com/science/article/B6TJK-4P940VB-1/2/f0539ed1a144078942ec2c6486808ffa

Buck, I., Foley, T., Horn, D., Sugerman, J., Fatahalian, K., Houston, M., Hanrahan, P., 2004. Brook for gpus: stream computing on graphics hardware. In: SIGGRAPH '04: ACM SIGGRAPH 2004 Papers. ACM, New York, NY, USA, pp. 777–786.

Correia, A. C. M., Couetdic, J., Laskar, J., Bonfils, X., Mayor, M., Bertaux, J., Bouchy, F., Delfosse, X., Forveille, T., Lovis, C., Pepe, F., Perrier, C., Queloz, D., Udry, S., Feb. 2010. The HARPS search for southern extra-solar planets. XIX. Characterization and dynamics of the GJ 876 planetary system. A&A 511, A21+.

Correia, A. C. M., Udry, S., Mayor, M., Benz, W., Bertaux, J., Bouchy, F., Laskar, J., Lovis, C., Mordasini, C., Pepe, F., Queloz, D., Mar. 2009. The HARPS search for southern extra-solar planets. XVI. HD 45364, a pair of planets in a 3:2 mean motion resonance. A&A 496, 521–526.

Gaburov, E., Bédorf, J., Portegies Zwart, S., 2010. Gravitational tree-code on graphics processing units: implementation in cuda. Procedia Computer Science 1 (1), 1113 – 1121, iCCS 2010.
URL http://www.sciencedirect.com/science/article/B9865-506HM1Y-4C/2/ee9cc0c6e9995324a31994e7e5595e9e

Gaburov, E., Harfst, S., Portegies Zwart, S., 2009. SAPPORO: A way to turn your graphics cards into a GRAPE-6. New Astronomy 14 (7), 630 – 637.

Gladman, B., Nov. 1993. Dynamics of systems of two close planets. Icarus 106, 247–+.

Hamada, T., Iitaka, T., Mar. 2007. The Chamomile Scheme: An Optimized Algorithm for N-body simulations on Programmable Graphics Processing Units. ArXiv Astrophysics e-prints (0703100).

Harris, C., Haines, K., Staveley-Smith, L., Oct. 2008. GPU accelerated radio astronomy signal convolution. Experimental Astronomy 22, 129–141.

Hill, G. W., 1878. Researches in the lunar theory. American Journal of Mathematics 1 (1), 5–26.
URL http://www.jstor.org/stable/2369430

Holman, M. J., Fabrycky, D. C., Ragozzine, D., Ford, E. B., Steffen, J. H., Welsh, W. F., Lissauer, J. J., Latham, D. W., Marcy, G. W., Walkowicz, L. M., Batalha, N. M., Jenkins, J. M., Rowe, J. F., Cochran, W. D., Fressin, F., Torres, et. al., 2010. Kepler-9: A System of Multiple Planets Transiting a Sun-Like Star, Confirmed by Timing Variations. Science, science.1195778.

Johnson, J. A., Howard, A. W., Bowler, B. P., Henry, G. W., Marcy, G. W., Wright, J. T., Fischer, D. A., Isaacson, H., May 2010a. Retired A Stars and Their Companions. IV. Seven Jovian Exoplanets from Keck Observatory. PASP 122, 701–711.

Johnson, J. A., Howard, A. W., Bowler, B. P., Henry, G. W., Marcy, G. W., Wright, J. T., Fischer, D. A., Isaacson, H., May 2010b. Retired A Stars and Their Companions. IV. Seven Jovian Exoplanets from Keck Observatory. PASP 122, 701–711.

Kokubo, E., Makino, J., Oct. 2004. A Modified Hermite Integrator for Planetary Dynamics. PASJ 56, 861–868.

Kokubo, E., Yoshinaga, K., Makino, J., Jul. 1998. On a time-symmetric Hermite integrator for planetary N-body simulation. MNRAS 297, 1067–1072.

Lee, M. H., Butler, R. P., Fischer, D. A., Marcy, G. W., Vogt, S. S., Apr. 2006. On the 2:1 Orbital Resonance in the HD 82943 Planetary System. ApJ 641, 1178–1187.

Portegies Zwart, S. F., Belleman, R. G., Geldof, P. M., Nov. 2007. High-performance direct gravitational N-body simulations on graphics processing units. New Astronomy 12, 641–650.

Raymond, S. N., Barnes, R., Veras, D., Armitage, P. J., Gorelick, N., Greenberg, R., May 2009. Planet-Planet Scattering Leads to Tightly Packed Planetary Systems. ApJL 696, L98–L101.

Rivera, E. J., Laughlin, G., Butler, R. P., Vogt, S. S., Haghighipour, N., Meschiari, S., Aug. 2010. The Lick-Carnegie Exoplanet Survey: a Uranus-Mass Fourth Planet for GJ 876 in an Extrasolar Laplace Configuration. ApJ 719, 890–899.

Schive, H.-Y., Tsai, Y.-C., Chiueh, T., 2010. Gamer: A graphic processing unit accelerated adaptive-mesh-refinement code for astrophysics. The Astrophysical Journal Supplement Series 186 (2), 457.
URL `http://stacks.iop.org/0067-0049/186/i=2/a=457`

Thompson, A. C., Fluke, C. J., Barnes, D. G., Barsdell, B. R., 2010. Teraflop per second gravitational lensing ray-shooting using graphics processing units. New Astronomy 15 (1), 16 – 23.
URL `http://www.sciencedirect.com/science/article/B6TJK-4WC4YHX-1/2/148b1e475460f2b9040ece847bc552ce`

Wright, J. T., Upadhyay, S., Marcy, G. W., Fischer, D. A., Ford, E. B., Johnson, J. A., Mar. 2009. Ten New and Updated Multiplanet Systems and a Survey of Exoplanetary Systems. ApJ 693, 1084–1099.